Estimation of scattering properties of lithosphere of Kamchatka based on Monte-Carlo simulation of record envelope of a near earthquake

I.R. Abubakirov and A.A. Gusev

Institute of Volcanology, Petropavlovsk-Kamchatsky, 683006 (U.S.S.R.)

(Received August 18, 1989; revision accepted May 1, 1990)

ABSTRACT

Abubakirov, I.R. and Gusev, A.A., 1990. Estimation of scattering properties of lithosphere of Kamchatka based on Monte-Carlo simulation of record envelope of a near earthquake. Phys. Earth Planet. Inter., 64: 52–67.

Several models which describe the intensity of single and multiply scattered waves radiated by an instant point source into a medium with uniformly dispersed scatterers and uniform absorption are reviewed. The model of multiple low-angle scattering (MLAS) is then considered and we show that in the realistic case of dominantly forward scattering one can employ the model to determine the mean free path l from pulse broadening of scattered waves. This fast ($\propto r^2$) pulse broadening leads to r^{-2} amplitude decay and can explain known fast-amplitude decay of short-range magnitude calibration curves and of peak acceleration attenuation laws.

Since analytical theory is lacking for an important case of scattered body waves at source distances around $r = l$, we employ the previously developed technique of Monte-Carlo simulation of a scattered wavefield to obtain a set of theoretical formulae and master curves. These enable us to estimate mean free path l in two independent ways: from intensity ratio of direct and scattered waves (l_A) and from pulse duration or retardation (l_T). In both cases, the estimates must depend only weakly on errors of Q determination. We applied the developed theory to the interpretation of records of earthquakes near Kamchatka recorded by frequency selecting ('ChISS') stations. For Shipunsky (SPN) station in the 1.5–6.0 Hz frequency range the estimates are $l_A \approx 150$ km, $l_T \approx 110$ km. In the 6–25 Hz range, l_A is decreasing, roughly as $f^{-0.65}$.

We could expect that improved theoretical coda shapes will resemble the observed ones, leading to accurate intrinsic Q estimates. This is not the case however, and our Q estimates depend in fact on the choice of lapse time window. This indicates that uniform medium models are insufficient for interpretation. We could demonstrate directly the depth dependence of l based on l_T estimates.

1. Introduction

The determination of absorptive and scattering properties of the medium based on scattered waves (first of all, coda) has become a routine procedure in recent years (e.g. Rautian et al., 1981; Jin et al., 1985; Gao et al., 1988; Sato, 1989, among others). The theoretical foundations of this approach cannot be considered, however, as absolutely definite. Usually the interpretation is carried out based on the models of single or multiple isotropic scattering in a medium with uniform distribution of random scatterers and uniform absorption. Almost all these assumptions can be (and more or less are) violated in nature. Three questions can be raised immediately. First, are the models employed fully adequate, given the assumptions on the medium? Secondly, how strong are real deviations from these assumptions? Thirdly, how can large errors be inflicted by these deviations in the estimates of medium properties? We shall address several aspects of these problems in the present paper.

The two problems of this kind to be discussed here will be the effects of multiplicity of scattering and of anisotropy of scattering indicatrix. Only

0031-9201/90/$03.50

when we take into account the multiplicity in an accurate way can we guarantee that no systematic errors are produced by inadequate approximate formulae; this can improve estimates of mean free path based on 'direct' wave to coda intensity ratio. As for anisotropy of scattering, it reveals itself in the shape of the peak of scattered energy, and has only a minor effect on coda. Estimates of mean free path and Q can be spoiled also by spatial non-uniformity of these parameters; however, here we discuss this important question only briefly.

Recently the 'energy flux' model (Frankel and Wennerberg, 1987) was proposed to describe a scattered wavefield at mean multiplicity of about one. We shall compare this model with other models in order to find out which model should be recommended for use in the interpretation.

When scattering is anisotropic (mainly forward), one can estimate its parameters not only from the 'direct' wave to coda intensity ratio but also from the pulse width (or retardation) of peak of scattered waves. This idea was proposed in Gusev and Lemzikov (1983) (see also the compressed version of this publication in Gusev and Lemzikov (1985)). (We shall often refer to the first paper, and thus the reference is abbreviated as GL83.) This approach was recently used by Sato (1989) based, however, on different theoretical foundations. Further we shall propose a new version of such an approach.

As a theoretical basis of formulae to be used in interpretation we used the results of numerical computations of envelopes of multiply anisotropically scattered waves. These computations were carried out using the Monte-Carlo technique and were described in Gusev and Abubakirov (1987); the more detailed version of some results of this paper is given here.

In the second part of the present paper we apply the developed approach to interpretation of records of earthquakes near Kamchatka. The results are of both methodological and geophysical interest.

2. Definitions and notations

We introduce here notations to be used below.

r source to receiver distance;

t observation (lapse) time, elapsed from the moment of radiation;

c body wave speed (S-wave speed in the following);

f, $\omega = 2\pi f$, Δf wave frequency (cyclic and angular) and half of band width;

W total source energy radiation in a narrow frequency band $(f - \Delta f,\ f + \Delta f)$;

$I(r, t)$ wave intensity for the same frequency band;

$I_c(t)$ asymptotic (coda) intensity; $I_c(t) \equiv I(0, t)$, $I(r, t) \to I_c(t)$ when $(ct/r) \gg 1$;

l, t^* mean free path and mean free time for the isotropic scattering (IS) case; $t^* = l/c$;

l_a, t_a^* mean free path/time for the anisotropic scattering (AS) case; $t_a^* = l_a^*/c$;

$\langle \cos\theta \rangle$ mean cosine of scattering angle θ, defined by $\langle \cos\theta \rangle = \int_\Omega \cos\theta p(\Omega) d\Omega / \int_\Omega p(\Omega) d\Omega$ where Ω is unit sphere and $p(\Omega)$ is the scattering indicatrix.

l_e, t_e^* is the effective mean free path/time and

$$l_e = l_a (1 - \langle \cos\theta \rangle)^{-1} \tag{1}$$

$$t_e^* = l_e / c$$

l_T, l_A, t_T^*, t_A^* empirical estimates of l_e and t_e^* based on pulse broadening (subscript T) and on intensity ratio of direct and scattered waves (subscript A);

Q, Q_c quality factor (non-elastic loss only) and its estimate from coda;

Q_{sc} quality factor due to scattering ($Q_{sc} = \omega t^*$);

q ratio $Q_s/Q = \omega t^*/Q$;

ρ dimensionless ('optical') distance for the IS case; $\rho = r/l$;

τ dimensionless lapse time (coincides with mean multiplicity of scattering) for the IS case; $\tau = t/t^*$;

ρ_a, ρ_e, τ_a, τ_e dimensionless distances and times for the AS case:

$$\rho_a = r/l_a,\ \rho_e = r/l_e,\ \tau_a = t/t_a^*,\ \tau_e = t/t_e^*.$$

t_m, τ_m retardation time of envelope peak measured from direct wave onset, and its dimensionless version, $\tau_m = t_m/t_e^*$;

$i(\rho, \tau)$, $i_c(\tau)$ dimensionless scattered intensity and its asymptotic version:

$$i(\rho, \tau) = \frac{l^2}{cW} I(r, t) \quad \text{for a 2-D case,}$$

$$i(\rho, \tau) = \frac{l^3}{cW} I(r, t) \quad \text{for a 3-D case,}$$

$$i_c \equiv i(0, \tau).$$

3. On theories of single and multiple isotropic scattering

The simplest model that describes a scattered wavefield is that of single isotropic scattering (SIS). It has almost obtained the status of the basic model in this field of research. When the SIS model is applied to near-earthquake records one usually assumes that the source is point-like, instant and as a rule isotropic; that scattering and absorptive properties of the medium are spatially uniform, and scattering is isotropic (that is, indicatrix is spherical). In this case, following Kopnichev (1975) and Sato (1977), we may write

$$I^{\mathrm{SIS}}(r, t) = \frac{W}{4\pi ctt^* r} \ln\left(\frac{ct + r}{ct - r}\right) \exp(-\omega t/Q) \tag{2}$$

$$I_c^{\mathrm{SIS}}(t) = \frac{W}{2\pi c^2 t^2 t^*} \exp(-\omega t/Q) \tag{3}$$

The second formula (Aki and Chouet, 1975) corresponds to $(ct/r) \to \infty$ and describes coda. Formulae (2) and (3) represent the first variant of the SIS model (let us denote it as SIS1) or Born approximation, when scattering losses of direct waves are ignored. If in (2) and (3) we replace Q^{-1} by $(Q^{-1} + Q_{\mathrm{sc}}^{-1})$ we arrive at the second variant of the SIS model, or SIS2. It is felt by some that the SIS2 model is more accurate than SIS1, and this is true for direct waves because additional losses are in fact accounted for. This does not seem to be the case for scattered waves. As was noted in (Aki and Chouet, 1975) the additional exponential factor can be compensated for by the contribution of waves of greater multiplicities, i.e. SIS2 describes single-scattered waves as such, but does not describe the full intensity. In fact the mentioned compensation is accurate for surface waves, and for body waves there is even some overcompensation. As a result, SIS1 gives more accurate predictions though SIS2 formulae seem to be more advanced.

For further discussion we consider it useful to pass to dimensionless variables ρ, τ and dimensionless intensity i. Formulae (2) and (3) now appear as

$$i^{\mathrm{SIS}}(\rho, \tau) = \frac{1}{4\pi\rho\tau} \ln\left(\frac{\tau + \rho}{\tau - \rho}\right) \exp(-q\tau) \tag{4}$$

$$i_c^{\mathrm{SIS}}(\tau) = \frac{1}{2\pi\tau^2} \exp(-q\tau) \tag{5}$$

The condition of applicability of the SIS model is now merely $\tau \ll 1$.

In the opposite case of high multiplicity ($\tau \gg 1$) the model of diffusion (isotropic) scattering (DIS) is valid (Wesley, 1965; Aki and Chouet, 1975). For body waves the model gives:

$$I^{\mathrm{DIS}}(r, t) = \frac{W}{c^2\left(\frac{4}{3}\pi tt^*\right)^{3/2}} \exp\left(-\frac{r^2}{\frac{4}{3}c^2 tt^*} - \frac{\omega t}{Q}\right) \tag{6}$$

$$I_c^{\mathrm{DIS}}(t) = \frac{W}{c^2\left(\frac{4}{3}\pi tt^*\right)^{3/2}} \exp(-\omega t/Q) \tag{7}$$

or, in the dimensionless form:

$$i^{\mathrm{DIS}}(\rho, \tau) = \frac{1}{\left(\frac{4}{3}\pi\tau\right)^{3/2}} \exp\left(-\frac{\rho^2}{\frac{4}{3}\tau} - q\tau\right) \tag{8}$$

$$i_c^{\mathrm{DIS}}(\tau) = \frac{1}{\left(\frac{4}{3}\pi\tau\right)^{3/2}} \exp(-q\tau) \tag{9}$$

The assumptions $\tau \ll 1$ and $\tau \gg 1$ are often unrealistic, and the problem of accurate accounting for multiplicity should be solved. An analytical approach to this problem for the 3-D case has led until now to only approximate results even for coda. Gao *et al.* (1983) found the formula for coda that accounts for waves with multiplicity up to the mth order. In dimensionless form it appears thus,

$$i_c^m(\tau) = \frac{1}{2\pi\tau^2}\left[\sum_{i=1}^{m} C_i\left(\frac{\tau}{2}\right)^{i-1}\right] \exp[-(q+1)\tau] \tag{10}$$

Values of coefficients C_i were calculated up to

$m = 7$. For $0 \leqslant \tau \leqslant 12$, eqn. (10) was approximated (with an error of up to 1%) by the expression

$$i_c^{GAO}(\tau) = \frac{1}{2\pi\tau^2}[1 + 1.23\tau \exp(0.33\tau)] \times \exp[-(q+1)\tau] \quad (11)$$

As can be seen from the following, there is not a wide range of validity for this result. Thus, at present accurate analytical formulae for intermediate τ are lacking even for coda. The Monte-Carlo technique, used by Gusev and Abubakirov (1987), gave the smooth curve for coda that interpolates between the two asymptotics (3) and (7). Its improved version is given below. For 2-D scattering (surface waves), the analogues of (3) and (7) were identical. Moreover, Shang and Gao (1988) and Zeng and Nie (1989) have shown analytically that the same general expression for coda is valid for any t. They also obtained the general (not asymptotic) formula, which in our notation looks like

$$I(r, t) = \frac{W}{2\pi t^* \sqrt{c^2t^2 - r^2}} \times \exp\left(\frac{\sqrt{c^2t^2 - r^2}}{ct^*} - \frac{t}{t^*} - \frac{\omega t}{Q}\right) \quad (12)$$

$$I_c(t) = \frac{W}{2\pi c t t^*} \exp(-\omega t/Q) \quad (13)$$

or, in the dimensionless form:

$$i(\rho, \tau) = \frac{1}{2\pi\sqrt{\tau^2 - \rho^2}} \exp\left[\sqrt{\tau^2 - \rho^2} - (q+1)\tau\right] \quad (14)$$

$$i_c(\tau) = \frac{1}{2\pi\tau} \quad (15)$$

Frankel and Clayton (1986) employed a technique of finite differences to simulate 2-D acoustic wave propagation through a random medium. While studying the domain $\tau \approx 1$, by this technique Frankel and Wennerberg (1987) found an inadequacy of the SIS2 model, and proposed instead a new one under the name 'energy flux model' (EFM). In the EFM, scattered energy is assumed to be uniformly distributed all over the region limited by a spherically expanding direct wave front; this leads to the expression (for body waves)

$$i_c^{EFM}(\tau) = \frac{1}{\frac{4}{3}\pi\tau^3}[1 - \exp(-\tau)] \exp(-q\tau) \quad (16)$$

The EFM was applied for interpretation.

The problem of accurate accounting for multiplicity is fully solved, however, for the 2-D case only; there are several models for the 3-D case, and one needs to choose one of them for interpretation.

4. Anisotropic scattering and the model of multiple low-angle scattering

Here we reject the second unrealistic assumption that is used in the SIS model, namely, the assumption of isotropic scattering. This assumption could be reasonable if a definite characteristic size of inhomogeneity existed, and this size was much less than the wavelength. For real Earth this seems improbable from general considerations. The SIS model is also in conflict with observations. As was noted in GL83, the observed 'direct' (in fact, forward-scattered) wave pulse becomes wider with 'distance'; this observation was confirmed by Sato (1989). In the SIS model, however, the direct wave pulse preserves its initial ('source') duration until it 'sinks' into scattered intensity.

Therefore it is useful to discuss whether, and how, the results for the isotropic case can be modified to describe anisotropic scattering with a (probably) forward-enhanced indicatrix. Let us begin with the case of large lapse time. For this case there is the following general result of transport theory (Ishimaru, 1978, chap. 9): the radiation field follows the DIS model with the effective mean free path value l_e. The condition of applicability of the DIS model is $\tau_e \gg 1$. At $\tau_a \ll 1$ the model of single anisotropic scattering is valid (e.g. Sato, 1982). In the range $t_a^* < t < t_e^*$ the specific case arises of multiple low-angle scattering (MLAS), first applied to the discussed seismological problem by Gusev and Lemzikov (1983, 1985) and Gusev and Abubakirov (1987) who based their work on Rytov (1966) and Chernov (1975). Strictly speaking the MLAS model is valid only

for a narrow indicatrix, but its real field of applicability is wider as one can see below from the results of numerical simulation.

The first important property of the MLAS model is that the pulse-like envelope shape is observed (contrary to the DIS case) but the pulse broadens (contrary to the SIS case). The second property is that pulse energy is nearly conserved with reference to the case of a homogeneous medium, because no back- or side-scattering arises. In reality, forward-scattered waves cannot be distinguished from direct waves, and we shall refer to the observed summary pulse as a 'direct' wave.

Broadening of a 'direct' wave pulse can be described based on a theory of a multitude of randomly curved rays (Rytov, 1966; Chernov, 1975). The variations of instant ray direction in this approach are treated as a continuous random walk over a unit sphere. Theory gives the following estimate for mean square distance r_{rms}^2 of ray point from its origin:

$$r_{\text{rms}}^2 = \langle r^2 \rangle = \frac{s}{D} - \frac{1}{2D^2}[1 - \exp(-2Ds)]$$

$$\approx s^2\left(1 - \frac{2Ds}{3}\right) \tag{17}$$

where $s = ct$ is current (cumulative) length of a curved ray, and D is a characteristic medium constant, called the 'ray diffusion coefficient'. Relation (17) leads to

$$s - r_{\text{rms}} \approx Ds^2/3 \tag{18}$$

Now let $t'_{\text{rms}} = (s - r_{\text{rms}})/c$ be rms time between (random) moment of wave arrival along shortest distance (along r) and fixed moment of its arrival along s. Let us change the viewpoint: assume r to be fixed, and s to be random, and introduce $t_{\text{rms}} = (s_{\text{rms}} - r)/c$. One can assume that the pulse width is near to t_{rms} and $t_{\text{rms}} \approx t'_{\text{rms}}$ (this fact can be proven accurately; the derivation is omitted here for brevity). Now (18) gives

$$t_{\text{rms}} \approx t'_{\text{rms}} \approx \frac{1}{3}\frac{Dr^2}{c} \tag{19}$$

The theory gives also the following estimate for mean cosine $\langle \cos \upsilon \rangle$ of full angle υ of deviation of ray direction from undisturbed (or mean) one:

$$\langle \cos \upsilon \rangle = \exp(-2Ds) \tag{20}$$

Formulae (19) and (20) are for continuous random walk. In the discrete case υ changes step-like in each act of scattering, and $\langle \cos \upsilon \rangle$ is defined by

$$\langle \cos \upsilon \rangle = \sum_{n=0}^{\infty} \langle \cos \upsilon_n \rangle P[k(s) = n] \tag{21}$$

where $\langle \cos \upsilon_n \rangle$ is mean cosine of full angle υ_n of deviation for scattering multiplicity n, $k(s)$ is scattering multiplicity for a cumulative ray length s, and $P[k(s) = n]$ is the probability of event $k(s) = n$.

Random variable $k(s)$ in the case of uniformly distributed scatterers has a Poisson's distribution, namely

$$P[k(s) = n] = \frac{(s/l_{\text{a}})^n}{n!} \exp(-s/l_{\text{a}}) \tag{22}$$

As for $\langle \cos \upsilon_n \rangle$, it is a multiplicative function of n (Landau and Lifshitz, 1976, section 127) so we may write

$$\langle \cos \upsilon_n \rangle = \langle \cos \theta \rangle^n \tag{23}$$

Now from (21), (22) and (23) one can derive

$$\langle \cos \upsilon \rangle = \exp[-s(1 - \langle \cos \theta \rangle)/l_{\text{a}}] \tag{24}$$

Or, taking (1) into account:

$$\langle \cos \upsilon \rangle = \exp(-s/l_{\text{e}}) \tag{25}$$

This important relation means that when the length of the ray approaches l_{e}, the initial ray direction is almost 'forgotten' so that $\langle \cos \upsilon \rangle$ decreases from about one to $\exp(-1)$. In other words, after dimensionless lapse time $\tau_{\text{e}} \approx 1$ the random wavefield becomes approximately isotropic. Comparing (25) with (20) one obtains

$$l_{\text{e}} = \frac{1}{2D} \tag{26}$$

From (26) and (19) one can derive

$$t_{\text{rms}} = \frac{1}{6}\frac{r^2}{l_{\text{e}}c} \tag{27}$$

which leads to

$$\tau_{\text{rms}} \equiv \frac{t_{\text{rms}}}{t_e^*} = \frac{\rho_e^2}{6} \tag{28}$$

This relation gives the general basis of estimation of t_e^* and l_e from the 'direct' wave retardation or pulse width. It is worth mentioning that in the case of the MLAS, the leading edge of the 'direct' wave pulse is very steep, and the trailing edge decreases rather slowly (turning into coda). The retardation time t_m for the peak of the pulse will be much lower, therefore, than rms retardation time t_{rms}. We can assume, however, that the quadratic form of the law is preserved for t_m also, so we can write

$$\tau_m \equiv t_m / t_e^* = \text{const} \cdot \rho_e^2 \tag{29}$$

The theory also relates $D = (2l_e)^{-1}$ with an autocovariation function (ACF) for fluctuations $\Delta n(\xi, \eta, \zeta) = [\langle c \rangle - c(\xi, \eta, \zeta)]/\langle c \rangle$ of refractive index n. Let

$$\begin{aligned} &\text{ACF}(x, y, z) \\ &\quad = \langle \Delta n(\xi, \eta, \zeta)\, \Delta n(\xi + x, \eta + y, \zeta + z) \rangle \\ &\quad = \langle \Delta n^2 \rangle N(x, y, z) \end{aligned} \tag{30}$$

so that $N(0, 0, 0) = 1$, and let $N(x, y, z) = \exp[-(x^2 + y^2 + z^2)/a^2]$, where a is a correlation distance. Then, for a ray along z

$$D = -\langle \Delta n^2 \rangle \int_0^\infty \partial^2 N / \partial x^2 \Big|_{x=y=0} \, dz = \frac{\sqrt{\pi}\, \langle \Delta n^2 \rangle}{a} \tag{31}$$

or,

$$l_e = \frac{a}{2\sqrt{\pi}\, \langle \Delta n^2 \rangle} \tag{32}$$

It should be noted that the same relation can be obtained also by the method of small perturbations (Chernov, 1975) in the approach based on an acoustic wave equation.

Based on a parabolic approximation (PA) for an acoustic wave equation Sato (1989) has shown how one can determine the combination $\langle \Delta n^2 \rangle / a$ from observations of average retardation time of a pulse peak. Further we shall calculate l_e estimates for both theories: MLAS based on ray or particle statistics and PA. It should be noted that quadratic law for $t_{\text{rms}}(r)$ is common for MLAS and PA (at $Q = \infty$).

5. Comparison of the results of Monte-Carlo simulation with other models, and derivation of calibration relations for interpretation

In our recent paper (Gusev and Abubakirov, 1987) we carried out the simulation of scattered wave envelopes using the Monte-Carlo technique. We shall give a brief summary here of previous results and include several new ones. The simulation procedure was based on transport theory which describes both particle propagation through a medium with scattering obstacles and radiation energy propagation through a randomly heterogeneous medium. The wavefield phase is supposed to be random, so that any diffraction or interference phenomena are ignored. The simulation consists of many repetitions of modelling of particle movement through the medium with scattering obstacles. The locations of scatterers and scattering angles are random and are never repeated. The time interval between scattering events is drawn as a pseudo-random number with exponential distribution. Unit values of mean free time t^* as well as of velocity c are assumed during simulation, so that modelling is carried out in the space of dimensionless variables ρ, τ. The direction of trajectory after scattering is either isotropic, or in order to simulate anisotropic scattering, is drawn according to gaussian indicatrix. In this case the value of angle θ is drawn from Rayleigh distribution with parameter δ, and the value of polar angle in a normal plane (that is normal to the 'old' direction) is drawn from uniform distribution in $(0, 2\pi)$. We modelled the spherically symmetrical case of isotropic point sources of 'particles' and of a uniformly scattering medium. No absorption was accounted for.

While simulating a trajectory we determined, at each model time moment $\tau_i = i\ \Delta\tau$, $i = 1, 2, \ldots$, in which the spherical layer (limited by radii $\rho_k = k\ \Delta\rho$ and $\rho_{k+1} = (k+1)\ \Delta\rho$, $k = 0, 1, 2 \ldots$) of the particle is located. The result of simulation is a set of values of normalized particle numbers, or dimensionless radiation energy density, for nodes of a grid in space (ρ, τ) (for the anisotropic case in space (ρ_a, τ_a)), with grid cell size $\Delta\rho \times \Delta\tau$ $(\Delta\rho_a \times \Delta\tau_a)$. Normalization is carried out through division by the number of simulated particles, and by

the volume of the spherical shell. In dimensionless variables, intensity is equal to energy density. Thus, we simulated the Green's function of one-speed non-stationary radiation transport equation for scalar waves, and the procedure described above gives direct estimates of $i(\rho, \tau)$, smoothed by a boxcar window of length $\Delta\rho$.

In Gusev and Abubakirov (1987) the simulated $i(\rho, \tau)$ function is presented as a function of τ, for a set of ρ values, for the isotropic case and for two computation runs for the anisotropic case, namely, for $\delta = 25°$ and $50°$. In these cases, $l_e = 5.2 l_a$ and $l_e = 1.69 l_a$, respectively. The coefficients are determined numerically through eqn. (1). The examination of simulated envelopes related obvious differences between isotropic and anisotropic cases of the kind described above: a narrow 'direct' wave peak of constant duration in the isotropic case (it can be observed in our simulation up to $\rho = 3$) and broadening of the 'direct' wave pulse in the anisotropic case.

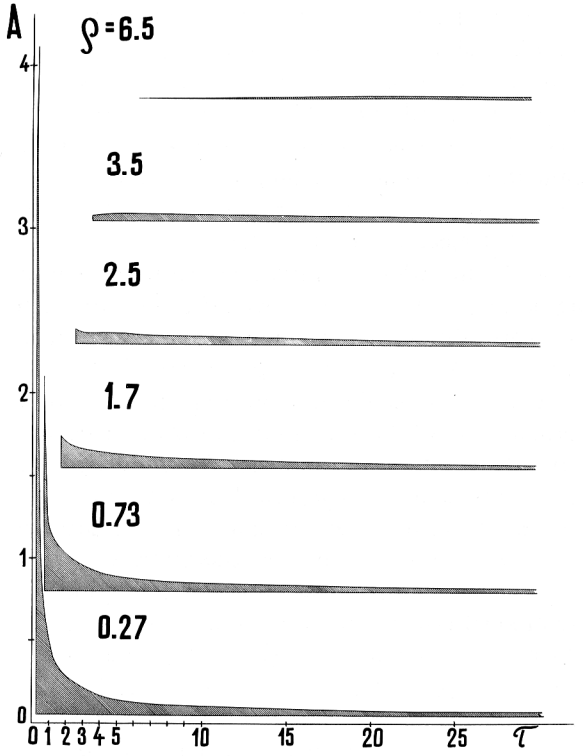

Fig. 1. Envelopes of scattered wave amplitude computed by Monte-Carlo technique for a case of isotropic scattering, for six values of dimensionless distance $\rho = r/l$. Abscissa is dimensionless time $\tau = ct/l$, ordinate is the amplitude in arbitrary units, the same for all plots. The plots are shifted vertically for better appearance.

Having rejected the isotropic model, of two anisotropic ones we choose the variant with $\delta = 50°$. The value $\delta = 25°$ (or less) was considered unacceptable, because at $\tau_a \gg \rho_a$ and $\tau_a < 3$ the envelope level 'sinks' clearly below the asymptotic i_c curve. This feature is not observed in reality (see Rautian et al., 1981). We explain this feature by a sharp decrease of the scattered wavefield level in the spatial region behind the trailing edge of the propagating 'direct' wave group. This region is 'lit' only by back-scattered radiation the level of which is unrealistically low at $\delta = 25°$ (and will go down further for narrower indicatrices). At $\delta = 50°$ such a feature is not seen in simulated envelopes. As no means is known today to determine δ values from empirical data, we consider the problem of optimal δ value estimation as unimportant. The value seems to lie in the range 40°–65°. At $t \geqslant 3t_e^*$ the difference between simulated envelopes for anisotropic and isotropic (with $t^* = t_e^*$) cases practically disappears, as would be expected from theoretical considerations for the diffusion case.

The log–log scale of discussed plots can make a clear realization of theoretical seismogram shapes difficult; therefore, in Fig. 1 we present a set of such curves, plotted with a common amplitude scale. They correspond to the isotropic case, and ρ varies from 0.27 to 6.5.

The simulated i_c curve for the isotropic case gives us a basis for interpretation of coda observations over the range between $\tau \ll 1$ and $\tau \gg 1$ (where the asymptotic SIS and DIS models are enough). The improved version of approximation of this curve can be written as

$$I_c(t) = \frac{W}{2\pi c^2 t^2 t^*}\left[1 + \left(\frac{27t}{16\pi t^*}\right)^x\right]^{1/2x} \times \exp(-\omega t/Q) \tag{33}$$

$$i_c(\tau) = \frac{1}{2\pi\tau^2}\left[1 + \left(\frac{27}{16\pi}\tau\right)^x\right]^{1/2x} \exp(-q\tau) \tag{34}$$

with $x = 1.10 \pm 0.025$.

To compare different scattering models it is useful to plot corresponding $i(\rho, \tau)$ as a function of ρ for a set of τ values. Unlike temporal envelopes discussed above, this mode of plotting of our results gives 'snapshots' of spatial distribution of the dimensionless radiation energy density. For the SIS model (see Fig. 2A) the functional form depends only on the ratio ρ/τ. EFM assumes that $i(\rho, \tau)$ is independent of ρ at any given τ; its predictions are seen in Fig. 2B. For the DIS model, valid for $\tau \gg 1$, $i(\rho, \tau)$ at given τ is a gaussian bell (Fig. 2C). This model predicts nonphysical (infinitely fast) waves arriving before the 'direct' wave. The integrated energy of these waves

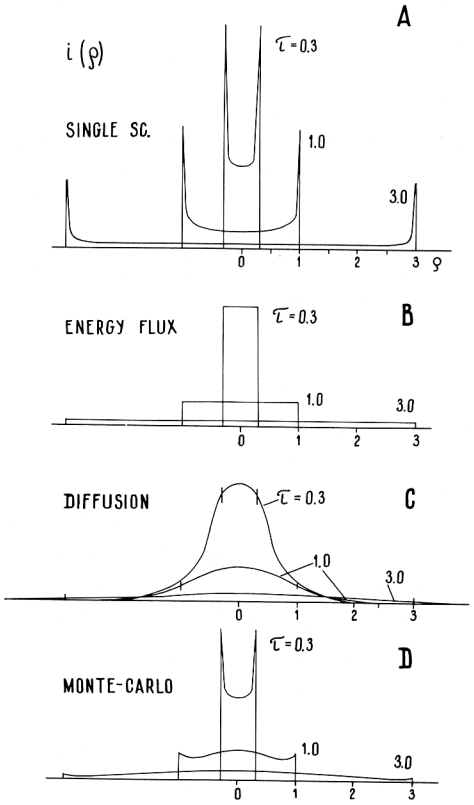

Fig. 2. 'Snapshots' of dimensionless intensity i of scattered waves at three moments of dimensionless time τ, for four models; isotropic scattering-single scattering (A), energy flux (B), diffusion (C), and a numerical model (D). The vertical scale is distorted, because with an accurate scale, plots for $\tau = 3$ would not be seen at all. Vertical dashes in C are the arrival moments of a direct wave; outside these points curves are unphysical.

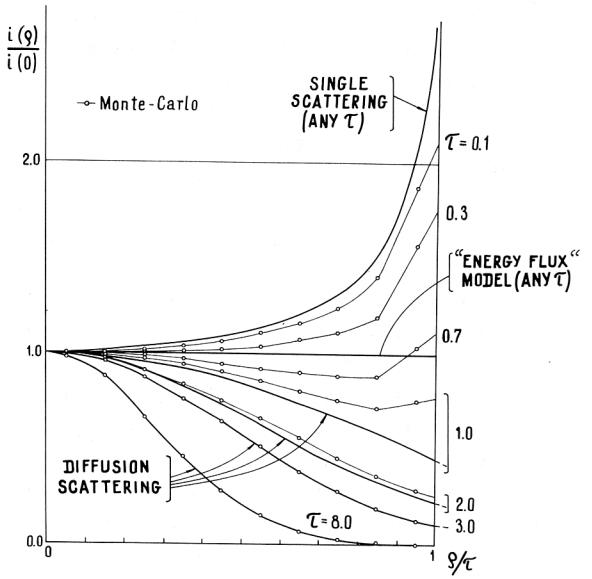

Fig. 3. Distance-dependence of dimensionless intensity i as in Fig. 2, but rescaled so that (1) direct arrival is fixed on new distance axis $\rho' = \rho/\tau$ at $\rho' = 1$ and (2) i values are normalized by their own value at $\rho = 0$ (i.e. i_c). ○———○ are Monte-Carlo estimates obtained by summation in windows of width $\Delta\rho' = 0.10$. For direct comparison, theoretical curves are also smoothed by a boxcar window of the same width.

is negligible however, for all τ such that the model is valid. Lastly, Fig. 2D presents the results of our simulation for the isotropic case (indicatrix type is unimportant here).

Comparing the last plot with three analytical models we can see that each model is qualitatively true for some range. To make the comparison more convenient we rescaled the curves of Fig. 2 in the following way. The distance axis was compressed so that with the new scale $\rho' = \rho/\tau$ arrival times always correspond to $\rho' = 1$, and i values were normalized so that normalized intensity is always equal to unity at $\rho' = 0$. The result can be seen in Fig. 3. Examination shows that from a quantitative aspect analytical formulae have only narrow ranges of applicability. The SIS model is reasonable up to $\tau \approx 0.4$, the DIS model to $\tau \geqslant 3$, and the EFM to $\tau \approx 0.5$–0.8.

These conclusions can be additionally confirmed by examination of Fig. 4, where $i_c(\tau)$ curves are plotted. One can see that at $\tau = 0.8$–3.0

the simulated relation $i_c(\tau)$ clearly deviates from any of the proposed analytical formulae. This gives us serious grounds for using the simulating $i_c(\tau)$ only while interpretating the empirical coda level. The second preference is a combination of the SIS1 and DIS models intersected at $\tau = 16\pi/27$. This idea was proposed previously in GL83. All models containing the $\exp(-\tau)$ factor seem to be inferior to these two.

The results of Monte-Carlo simulation enable us also to construct master curves for interpretation of data on the basis of the pulse shape (width and/or retardation). Here we choose the retardation time τ_m of envelope peak as a main parameter. Generally speaking, the rms retardation (or some other measure) may be a better choice. Our decision was based on two reasons: first, τ_m estimates were easy to obtain by our Monte-Carlo technique and, secondly, the results will be ready to apply in visual interpretation of photo records.

The smoothed simulated relation $\tau_m(\rho_e)$ for $\delta = 25°$ and $50°$ is presented in Fig. 5. The analytical relation for DIS model

$$\tau_m = \rho_e^2/2 - \rho_e \qquad (35)$$

is plotted also (for the case $Q = \infty$), and the

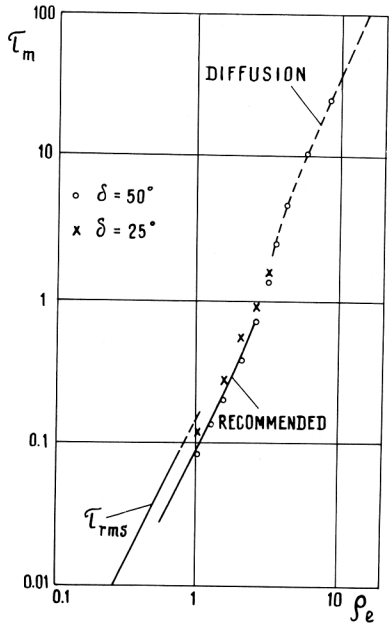

Fig. 5. Dimensionless retardation time τ_m between direct wave arrival and peak of scattered intensity, as a function of dimensionless distance ρ_e. τ_{rms} is rms retardation of scattered waves according to the MLAS model. The dashed line is a theoretical one for the diffusion model. Symbols are Monte-Carlo estimates. The continuous line is recommended to be used in interpretation. Extrapolation of this line is not secure.

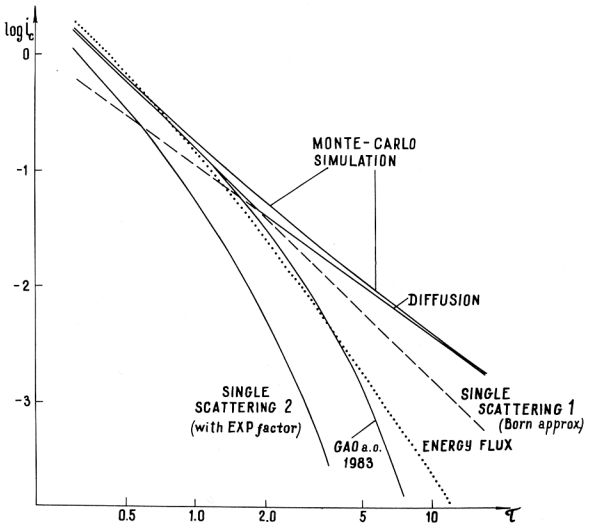

Fig. 4. Dimensionless coda intensity $i_c(\tau)$ according to different models of scattering.

relation (28) for τ_{rms} as well. τ_{rms} is greater than τ_m as expected.

The accuracy of our present Monte-Carlo estimates of τ_m is low at $\rho_e < 3$ (not better than 20% at $\rho_e = 1.5$), but two preliminary conclusions can be arrived at. First, DIS predictions fully coincide with simulation results at $\rho_e > 3$. Second, the trend $\tau_m \sim \rho_e^2$ which was expected from the MLAS model at $\rho_e < 1$ seems to be extended up to $\rho_e = 2.0$–2.5. At $\rho_e < 1$ our estimates can suggest the smoothed and somewhat extrapolated relation $\tau_m(\rho_e)$ which is plotted in Fig. 5 as a first approximation. In the range $\rho_e = 0.5$–2.0 it follows a formula

$$\tau_m = 0.10\rho_e^2 \qquad (36)$$

or in dimensional variables

$$t_m = 0.10r^2/(cl_e) \qquad (37)$$

This leads to the following estimate of l_e:

$$l_T = 0.10r^2/(ct_m) \tag{38}$$

Based on this formula we can now use the observed retardation time–distance relation for the determination of scattering properties of the medium. The relation (38) can and will be improved when simulations with better resolution along the τ axis and taking absorption into account are carried out.

Based on PA for the acoustic wave equation and using gaussian ACF for random velocity inhomogeneities Sato (1989) obtains (at $Q = \infty$) the following relation:

$$t_m = \frac{\sqrt{\pi}\langle \Delta n^2 \rangle r^2}{3ac} \tag{39}$$

Combining this with (32) gives

$$t_m = \tfrac{1}{6} r^2/(cl_e) \tag{40}$$

and l_e estimate of the form:

$$l_T^{PA} = \tfrac{1}{6} r^2/(ct_m) \tag{41}$$

This estimate is 1.67 times greater than (38); this difference demonstrates a real difference between the predictions of the two theories and will be the object of further study.

Sato (1989) also takes absorption into account while calculating theoretical estimates of t_m. The effect of this factor is real, but at $\rho_e < 1.5$ it is relatively weak, and we think that it can be neglected in the first approximation.

6. Determination of the S-wave mean free path in the lithosphere of Kamchatka

The theoretical relations of the previous section were applied to an interpretation of real data. We used observations of frequency selecting ('ChISS') stations Shipunsky, (SPN), Petropavlovsk (PET) and Topolovo (TOP) operated in Kamchatka in 1966–1972, under the supervision of S.A. Fedotov and S.A. Boldyrev. The stations were equipped with 5-s vertical instruments of the S5S type; their output, proportional to velocity, was passed through seven octave band-pass filters with central frequencies of about 0.4, 0.8, 1.5, 3, 6, 12 and 25 Hz, and then photo-recorded.

The interpretation technique employed is in fact an improved version of the technique described in GL83 (see also Gusev and Lemzikov, 1985). While designing the processing procedure in GL83 the authors considered it important to employ a method of estimating l that is more or less independent of possible errors of estimation of Q. Several approaches were studied. The first (main) one is more traditional and based on intensity ratio of direct and scattered waves. Its new element is that this ratio is estimated at identical lapse time, so that Q-dependent factors cancel. We shall use this approach further.

Another very rough technique proposed in GL83 was based on the theory that at traveltimes of about t^* the 'direct' wave pulse must 'sink' in diffuse scattered background. This general idea seems reasonable even today, but strict formulation of the technique is difficult and we shall not try to use it again. It is worth mentioning, however, that l estimates obtained in such a simple way reasonably agree with supposedly more accurate estimates obtained by the first technique in GL83 or in the present paper.

The third technique described in GL83 was not fully Q-independent and will not be discussed here. In addition, the technique was proposed to estimate t^* from pulse broadening of 'direct' S-waves. We shall use the improved versions of the first and the last approaches further, and begin with the first one.

In order to compare levels of direct wave and coda at the same lapse time the following empirical functions were determined from observations:

$$a_c(t) = A_c(t)/A_c(100) \tag{42}$$

—coda amplitude normalized by its value at the lapse time $t = 100$s, and

$$a_s(t) = A_{0s}(t)/A_c(100) \tag{43}$$

—reduced S-wave amplitude normalized in a similar way. The reduction of S-wave amplitude was carried out to compensate for pulse broadening, and individual A_{0s} values used in the compilation of (43) were computed as $A_{0s} = A_s\sqrt{d/d_0}$, where

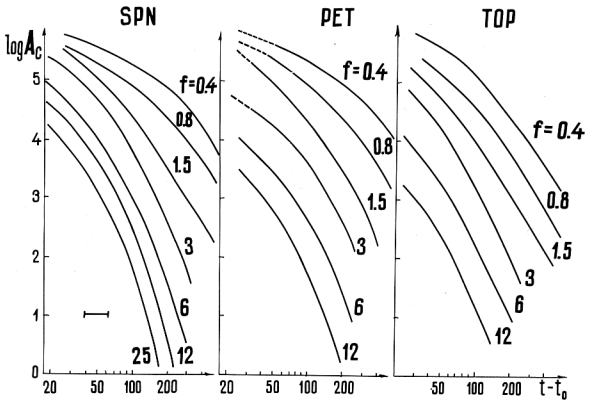

Fig. 6. Empirical coda amplitude envelopes in seven octave frequency bands for three Kamchatka stations (space location see insert in Fig. 7).

d_0 is the visual duration of pulse response of band filter (that is minimal duration), and d is the observed S-wave pulse duration. Relation (42) is merely the experimental coda envelope. Seven $a_c(t)$ curves for three stations were determined in a mainly traditional way (see GL83 for details) and plotted in Fig. 6. Relation (43) for SPN was presented in GL83; the plot for PET is similar. Not enough data were collected for TOP to construct an $a_s(t)$ curve.

From $a_c(t)$ and $a_s(t)$ functions one can pass to t^* and l estimates in two steps. At the first step one can go from amplitude curves to intensities and their ratio, and at the second step, from this ratio to t^* and l. Let us begin with the theory for the second step. The direct wave intensity I_d in the SIS2 model (in fact, generally), can be written as

$$I_d(r) = \frac{W}{4\pi c^2 t_d^2 d_s} \exp\left(-\frac{\omega t_d}{Q} - \frac{t_d}{t^*}\right) \qquad (44)$$

where d_s is the duration of assumedly boxcar radiation pulse, r-distance and $t_d = r/c$. The coda wave intensity I_c follows (33), and we assume here $t_d = t$ in (44). Now introducing the dimensionless ratio $B = tI_c/(d_s I_d)$, then (33) and (44) give

$$B = B(\tau) = 2\tau \exp(\tau)\left[1 + \left(\frac{27}{16\pi}\tau\right)^x\right]^{1/2x} \qquad (45)$$

with $x = 1.10 \pm 0.025$. Thus, B depends only on τ, and from (45) one can find inverse function $\tau = \tau(B)$, and then $t^* = t/\tau(B)$.

Now we see that at the first step we must fix t and determine the ratio $I_c/(d_s I_d)$. As for t, its choice is dictated by the narrow region where we managed to determine $a_s(t)$ and $a_c(t)$ simultaneously and with reasonable accuracy, so $t = 20$–25 s. Now consider the determination of intensities. To determine the S-wave intensity from known (squared) amplitudes one needs to introduce several corrections to account for: the difference between the actual S-wave pulse envelope and assumed boxcar envelope; ChiSS band-width; the difference between visual and effective pulse duration; the difference between rms amplitude and extreme peak amplitude, which depends on the number of peaks. Similar corrections should be included for scattered waves. For detailed discussions of listed corrections one should refer to GL83. In the case of S-waves it is more convenient to estimate directly 'energy', or the integral of I over the pulse duration, which equals $d_s I_d$. Therefore, B values were determined from empirical data in the way described and t^* (and $l = 3.5$ km $s^{-1}t^*$) with them.

As will be demonstrated further, for lower frequency bands of 0.4 and 0.8 Hz the surface wave scattering model is more correct and should be preferred. In this case one should use (13) instead of (33), and should modify (44) accordingly. An analogue of (45) for this case is

$$B = B(\tau) = \tau \exp(\tau) \qquad (46)$$

which was employed in practical computation.

Experimental t^* estimates t_A^* obtained in this way (from the intensity ratio) correspond to t_e^* estimates, because scattering is in fact anisotropic. Values of t_A^* and $l_A = 3.5$ km $s^{-1}t_A^*$ are given in Table 1 for SPN and in Table 2 for PET, with other relevant data. Their accuracy is about 30–50%. Differences between three frequency bands in the range 1.5–6.0 Hz are not significant and an average estimate of $l_A \approx 150$ km was obtained for SPN. In the 6–25 Hz range l_A is decreasing roughly as $f^{-0.65}$.

To estimate t_e^* and l_e from pulse shape data we used data of GL83 on the dependence of visual S-wave pulse duration on distance. For 1.5, 3.0

TABLE 1

Estimates of medium parameters under SPN based on scattering models of surface waves ($f = 0.4$ and 0.8) and body waves (other frequencies)

Parameter	Central frequency of band filter f (Hz)						
	0.4	0.8	1.5	3	6	12	25
t (s)	25	25	25	20	20	20	20
log a_c	0.55	0.64	1.13	1.58	1.94	2.10	2.39
log a_s	0.95	0.70	1.41	2.28	2.71	2.87	3.18
log B	−0.27	0.53	0.48	0	0.19	0.53	0.93
t_A^* (s)	68	22.50	37	59	44.30	27.80	17.80
l_A (km)	238	79	130	207	155	97	62
t_T^* (s)	–		31	34	29	–	–
l_T (km)	–		110	120	100	–	–
t^* (s) [a]	–		43	43	43	27	17
l (km) [a]	–		150	150	150	95	60
$Q_c(t = 50–80$ s)	180	200	200	315	500	825	1600

[a] Values assumed for all stations while calculating Q_c for 3-D cases.

and 6.0 Hz bands estimates were found for the parameter p in the relation

$$t_v = p(r/c)^2 \tag{47}$$

where t_v is the d value corrected for pulse broadening by band filter (this correction is in fact important for the 1.5 Hz band only). One can assume as a first approximation that $t_m = 0.5t_v$, then (37) gives $t_T^* = 0.2/p$. Values of t_T^* and $l_T = 3.5$ km s$^{-1} t_T^*$ for SPN are also given in Table 1. Differences between the three frequency bands are small, and the common estimate $l_T \approx 110$ km was obtained. Data from hypocentral distance range 40–100 km were used. Taking real accuracy into account, the agreement between l_A and l_T values is reasonable. Estimates of l by both techniques are plotted in Fig. 7.

Sato (1989) used parabolic approximation to study pulse broadening. For Ashio station in Japan an estimate $\log(\langle \Delta n^2 \rangle / a) = -2.98 \pm 0.32$ for five frequency bands from 2 to 32 Hz and for hypocentral distance range of 80–300 km was obtained. The value −2.98 through (32) leads to the estimate $l_T^{PA} = 270$ km which corresponds to $l_T = 162$ km. An estimate for l_A was previously found for the neighbouring region to be 83 km (Sato,

TABLE 2

Estimates of medium parameters under PET and TOP based on scattering models of surface waves ($f = 0.4$ and 0.8) and body waves (other frequencies), (t value is 25 s)

Parameter	Central frequency of band filter f (Hz)					
	0.4	0.8	1.5	3	6	12
Station PET						
log a_c	0.52	0.73	1.18	1.08	1.38	–
log a_s	0.60	0.65	1.17	1.55	2.10	–
log B	0.38	0.79	1.06	0.56	0.43	–
t_A^* (s)	26.70	17.30	19.60	33.5	39.50	–
l_A (km)	93	61	69	117	138	–
$Q_c(t = 50–80$ s)	220	150	135	560	640	870
Station TOP						
$Q_c(t = 50–80$ s)	80	120	185	250	415	720

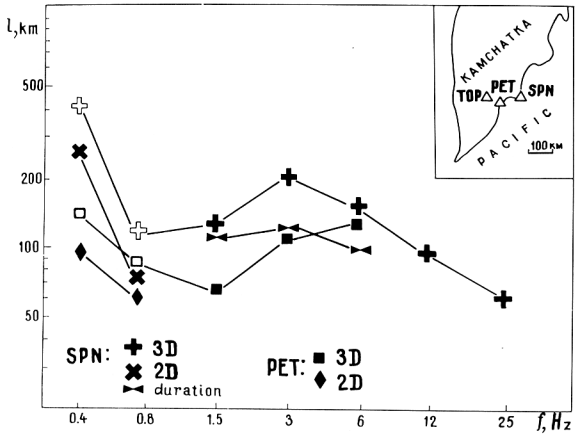

Fig. 7. Effective mean free path l_e estimates for Kamchatka, at different frequency bands. For SPN and PET l_A estimates are given (from amplitudes), for body wave (3-D) and surface wave (2-D) scattering. For SPN, l_T estimates (from pulse broadening) are also given. The insert illustrates station location.

1978). Thus, l_A and l_T estimates for Japan as well as for Kamchatka are comparable with one another and for the two regions.

There are three kinds of complications related to l_e estimates of the l_T type. First, one should remember that for crustal rays, representation of energy propagation by surface waves is a well-known alternative model to body wave scattering. It should be noted, however, that in island arc regions no Lg wave is observed and no systematic short-period surface wave train can be seen. For this reason the body wave scattering model of energy propagation is applicable. The detailed comparison of capability of the two models to describe real data is left for the future.

Secondly, there is a possibility of dependence of intensity of forward-scattering on local ray angle of incidence. In a random medium with a tendency to layering, scattering can be stronger for near-horizontal rays as compared with near-vertical rays. Phenomena of this kind are not easy to observe. They can imitate depth dependence of l_e discussed below.

Last but not least is the problem of vertical non-uniformity of scattering properties of the medium. For a given angle of incidence at the receiver, the greater the distance, the greater the proportion of time energy that propagates in deep 'low-turbidity' layers (up to the turning point of the ray). The same is true when r is constant but source depth is increased. Hence, the observed $t_m(r)$ dependence can be slower than the expected r^2 law, and l_e estimates can depend on distance and/or source depth. This possibility was considered so important that an additional study was carried out.

We took S-wave groups (visual periods 0.2–0.8 s) of local earthquakes on photo-records of conventional horizontal short-period electromagnetic seismographs (period 1.2s) at Shipunsky station as initial data. Use of broad-band records (in contrast to band-filtered ones) is justified as soon as our previous l_e estimates are stable in the range of 1.5–6.0 Hz. Data were selected with hypocentral distance between 70 and 200 km. We measured the retardation of S-wave peak amplitude shortest on the two horizontal components with respect to either (1) visual or (2) computed S-wave onset. The results for versions (1) and (2) almost coincide. Two groups of data (the total number of events ≈ 50 in each group) were formed: the first (a) with depth $h = 0$–35 km and the second (b) with $h = 35$–150 km. The empirical $t_m(r)$ relationship was estimated to be: $(1.95 \pm 0.23)(r/100)^{1.51 \pm 0.34}$ (a) and $(1.07 \pm 0.08)(r/100)^{0.94 \pm 0.22}$ (b) (in s).

Based on the average t_m value for typical $r =$ 100 km, l_T estimates from (38) are: $l_T(a) = 150$ km, $l_T(b) = 270$ km. Thus, depth dependence of scattering properties seems to be prominent.

The results above make one realize clearly to which volume of medium each estimate corresponds. l_A estimates are based on data for lapse time 20–25 s. Assuming SIS this leads to a one-way distance of 35–40 km; thus the value $l_A = 150$ km (for 1.5, 3.0 and 6.0 Hz) corresponds to a hemisphere of the 35–40 km radius under Shipunsky. As in GL83 mainly 'crustal' (depth 0–40 km) events were studied with S–P of 5 to 15s, our estimate $l_T = 110$ km for ChISS data corresponding to the disk-like volume of radius of about 100 km and thickness of 40 km. The estimate $l_T = 150$ km for case (a) of broad-band data corresponds to the same volume. Estimate $l_T = 270$ km for the case (b) corresponds to the hemisphere of 100 km

radius. Thus, three estimates for upper layer agree well, and the last, greater value indicates much lower turbidity of deeper Earth layers.

7. S-wave absorption in the lithosphere of Kamchatka

In the case of surface wave scattering (13) and also for body waves when SIS1 (3) or DIS (7) models are valid one need not know the l (in fact l_e) values when attempting to obtain Q estimates from coda. In practice, τ (in fact τ_e) values between 0.5 and 3.0 are typical, hence one should use theory for body waves (33). To do this, one needs to estimate l in advance. In the following computations for all stations we fixed a set of l and t^* values which is given in Table 1. At a given t^*, the envelope shape follows (33), where Q is now the only free parameter (but amplitude is level).

To obtain Q (Q_c) estimates from coda we constructed a set of curves (33) with Q_c as a parameter. This set of master curves in log–log scale was compared with experimental curves of Fig. 6, and the best-fitting curve was chosen. The degree of fit differs from different bands and stations. Generally, one cannot fit a theoretical curve to the empirical one in the whole range of lapse time. Therefore we estimated Q_c for a set of successive t intervals of log duration equal to 0.2. These estimates were ascribed to the log centre of each interval. Examples of empirical relations $Q_c(t)$ obtained in this way are plotted in Fig. 8 for two frequency bands for three stations. For the 0.4 and 0.8 Hz bands Q_c estimates were negative. We considered this fact as an indication that the body-wave scattering model is incorrect, and repeated interpretation in the context of the surface wave scattering model.

Examination of Fig. 8 shows that the use of the theoretically correct $I_c(t)$ relation does not lead to the agreement of Q_c estimates at different lapse times. Therefore the theoretical model used is, strictly speaking, inadequate, and Q_c estimates may be doubtful. One can consider them, however, as more or less realistic in cases where the Q_c estimate weakly depends on t over a wide enough t range.

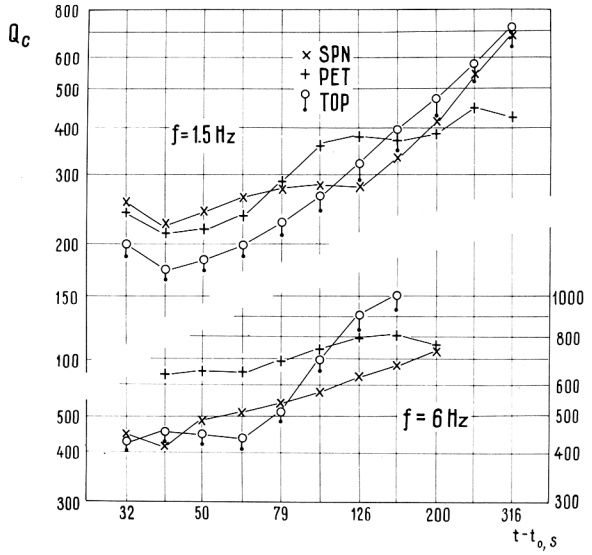

Fig. 8. S-wave quality factor Q_c estimated from coda for two frequency bands as a function of lapse time moment corresponding to the log centre of the lapse time window used for Q_c determination. The window length was 0.2 in log units (e.g. 50–80 s). Coda shape was assumed to follow (33).

Of interest is a comparison of described estimates with those obtained by the SIS1 model. They were computed for TOP station, and are also shown in Fig. 8. One can see that differences are not large, from 10% at $t = 40$s up to 30% at $t = 300$s; Q_c estimate by SIS1 is always below that produced by the full theory. One can also see in Fig. 8 that Q_c estimates from different stations tend to get closer at large t. This is reasonable from the viewpoint of general assumptions on coda formation.

Frequency dependence of Q_c is presented in Fig. 9 for all stations and frequencies where we had enough data and for the lapse time interval $t = 50$–80s which generally gives the most stable estimates. This dependence for body waves generally follows the usual relation $Q_c(f) = Q_0 f^x$ (for frequencies higher than about 1 Hz) with $x = 0.7$–0.8 and $Q_0 \equiv Q_c(1\text{ Hz}) = 160$–$180$. These Q_c values can be associated with a half-sphere of radius 100–150 km around the station. For reference we compiled several published Q_c estimates (using

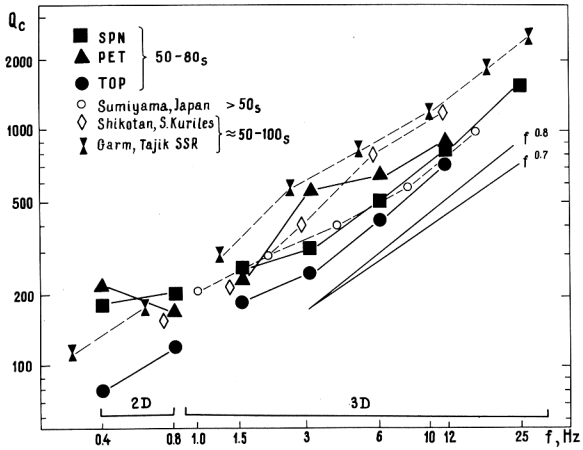

Fig. 9. Q_c estimates for lapse time window 50–80 s, for different frequency bands, for three Kamchatka stations. The surface wave model was used for 0.4 and 0.8 Hz, and the body wave model for others. Estimates for Japan, South Kuriles and Garm are added for comparison; they all correspond roughly to the same lapse time window.

the SIS1 model) with specified lapse time interval which was near to the interval we used (Akamatsu, 1980; Rautian et al., 1981). Estimates of Rautian et al. (1981) were somewhat modified based on original a_c curves.

It is worth mentioning that advanced estimates of l_e and Q_c presented here are not very far from the initial estimates of Gusev and Lemzikov (1983) who used more primitive versions of the approach described.

8. Discussion and conclusions

In the theoretical part of this paper we present an approach to the modelling of scattered waves and interpretation of observations which is based on particle or ray statistics. Such an approach is clearly more primitive than the full wave theory, but it enables us to solve certain simple problems of intensity. We studied in some detail the case of a uniformly scattering medium, and proposed two independent ways to estimate mean free path—from 'direct' to scattered wave intensity ratio and from pulse broadening of the direct wave.

This pulse broadening phenomenon was discussed above based on a multiple low-angle scattering model. One result of this model is of general interest, as it may clarify some old apparent paradoxes of observational seismology related to amplitude decay of near-earthquakes. In fact, approximate energy conservation at relatively short distances combined with r^2 pulse broadening leads to r^{-2} amplitude decay of body waves. This theoretical result can easily explain the obvious contradiction between fast-amplitude decay expressed in magnitude calibration curves and peak acceleration attenuation laws (typically r^{-x}, with $x = 1.7–2.3$) on one hand, and the general success of seismic moment determination based on the assumed r^{-1} law for spectral amplitude, on the other hand. It should be noted that such a contradiction can be expected and in fact exists for small and moderate earthquakes only, when source duration is small relative to scattering-related broadening. For larger events pulse duration is determined by source duration which is distance-independent, hence amplitude decay becomes much nearer r^{-1}.

We applied the theoretical results to interpretation of real data and obtained two rows of mean free path estimates which generally agree. But an attempt to estimate Q for S-waves from coda in frames of the discussed model was only partly successful; the dependence of Q estimates on the lapse time window seems to demonstrate the deviations of a real medium from the assumed simple model and casts some doubts on the accuracy of our l estimate. Generally speaking, model inadequacy may lead to systematic and mutually compensated errors in Q and l. Particularly dangerous is the rather realistic case when Q and l both increase with depth (case discussed in GL83). Here we have shown that l increase with depth is real. This increase leads to growth of 'radiative' losses, which add to intrinsic losses thus decreasing Q estimates based on the uniform medium model. Construction of interpretation procedures for such cases is an important task for the future.

In view of problems of the type described above the gain in accuracy obtained by our application of a more advanced theoretical model for coda waves in a uniform medium may be considered of secondary value. We consider it to be, however, important in principle and thus worthy of special remark.

The technique of l determination through pulse retardation measurement (giving an l_T estimate) developed above seems to have at least two advantages. First, it gives us values which are almost Q-independent, and fully independent of traditional l_A estimates providing an opportunity of mutual checking. Secondly, l_T estimates are much more effective for study of l structure because the main contribution to l is produced by a relatively narrow tube along the ray, and not by a large half-sphere as for l_A. Therefore, a perspective is obtained from the tomographic approach which is almost impossible with l_A estimates.

In conclusion, for many problems of short-period seismology where phase information and diffraction phenomena are not of key importance, an energy transportation approach and its realization through the Monte-Carlo technique can provide results that are useful means of interpretation.

References

Akamatsu, J., 1980. Attenuation property of coda parts of seismic waves from local earthquakes. Bull. Disas. Prev. Res. Inst., Kyoto Univ., 30: 1–16.

Aki, K. and Chouet, B., 1975. Origin of coda waves: source, attenuation and scattering effects. J. Geophys. Res., 80: 3322–3342.

Chernov, L.A., 1975. Volny v Sluchaino-Neodnorodnyh Sredah (Waves in Randomly Inhomogeneous Media). Nauka, Moscow, 170 pp. (In Russian.)

Frankel, A. and Clayton, R.W., 1986. Finite difference simulations of short-period seismic waves and models of crustal heterogeneity. J. Geophys. Res., 91: 6465–6489.

Frankel, A. and Wennerberg, L., 1987. Energy-flux model of seismic coda: separation of scattering and intrinsic attenuation. Bull. Seismol. Soc. Am., 77: 1223–1251.

Gao, L.S., Biswas, N.N., Lee, L.C. and Aki, K., 1983. Effects of multiple scattering on coda waves in three-dimensional medium. PAGEOPH, 121: 3–15.

Gao, L., Hua, Z. and Li, R., 1988. Estimation of mean free path of S-waves under Beijing area by means of both intensity and decay of codas. Acta Seism. Sinica, 1: 13–29.

Gusev, A.A. and Abubakirov, I.R., 1987. Monte-Carlo simulation of record envelope of a near earthquake. Phys. Earth Planet. Inter., 49: 30–36.

Gusev, A.A. and Lemzikov, V.K., 1983. Estimation of shear wave scattering parameters in the crust and upper mantle of Kamchatka by observations of the 'Shipunsky' station. Vulcanol. Seismol., 1: 94–108 (in Russian. See Engl. Transl. in Volcanol. Seismol., 5: 97–114).

Gusev, A.A. and Lemzikov, V.K., 1985. Properties of scattered elastic waves in the lithosphere of Kamchatka: parameters and temporal variations. Tectonophysics, 112: 137–153.

Ishimaru, A., 1978. Wave Propagation and Scattering in Random Media, Vol. 1. Academic Press, New York.

Jin, A., Cao, T. and Aki, K., 1985. Regional change of coda Q in the oceanic lithosphere. J. Geophys. Res., 90: 8651–8659.

Kopnichev, Y.F., 1975. A model of generation of the tail part of the seismogram. Dokl. Akadem. Nauk SSSR, 222: 333–336 (in Russian).

Landau,. L.D. and Lifshitz, E.M., 1976. Statisticheskaja Fizika (Statistical Physics). Nauka, Moscow, 583 pp. (in Russian.)

Rautian, T.G., Khalturin, V.I., Zarikov, M.S., Zemtsova, A.G., Prockurin, A.P., Pustovitenko, B.G., Pustovitenko, A.N., Sinelnikova, L.G., Filina, A.G. and Sengelia, I.S., 1981. Experimental Studies of Seismic Coda. Nauka, Moscow, 142 pp. (In Russian.)

Rytov, S.M., 1966. Vvedenie v Statisticheskuyu Radiofiziku (An Introduction to Statistical Radiophysics). Nauka, Moscow, 404 pp. (In Russian.)

Sato, H., 1977. Energy propagation including scattering effects. Single isotropic scattering approximation. J. Phys. Earth, 25: 27–41.

Sato, H., 1978. Mean free path of S waves under the Kanto district of Japan. J. Phys. Earth., 26: 185–198.

Sato, H., 1982. Coda wave exitation due to nonisotropic scattering and nonspherical source radiation. J. Geophys. Res., 87: 8665–8674.

Sato, H., 1989. Seismic wave envelope broadening in the randomly inhomogeneous structure beneath south-eastern Honshu, Japan. J. Geophys. Res., submitted.

Shang, T. and Gao, L., 1988. Transportation theory of multiple scattering and its application to seismic coda waves of impulse source. Scientia Sinica, Ser. B, 31: 1503–1514.

Wesley, J.P., 1965. Diffusion of seismic energy in the near range. J. Geophys. Res., 70: 5099–5106.

Zeng, J. and Nie, Y., 1989. The effects of single and multiple scattering on coda waves for local earthquakes. Acta Seism. Sinica, 11: 11–22 (in Chinese).